Ocean variability drives a millennial-scale shift in South Pacific hydroclimate

Check for updates

Mark Peaple [1,6] ✉, Daniel T. Skinner [2,3,6], Gordon N. Inglis [4], Manoj Joshi [2,3], Peter Langdon [1], Adrian J. Matthews [3,5], Timothy J. Osborn [2,3] & David Sear [1]

The South Pacific Convergence Zone is a band of intense austral summer rainfall in the tropical Pacific. Changes in the South Pacific Convergence Zone are linked to Pacific sea surface temperatures on decadal timescales, but its behaviour and impacts over longer timescales remain poorly understood due to limited proxy records and model uncertainties. We combine new plant wax hydroclimate records with existing proxy evidence and climate model simulations to investigate South Pacific Convergence Zone changes over the past 1500 years. Our findings indicate that between 1000 and 200 years ago, the eastern South Pacific Convergence Zone became wetter while the western part became drier. Model simulations suggest that these centennial-scale changes were driven by Pacific sea surface temperature gradients. This eastward shift coincides with Polynesian colonisation, implying hydroclimate shifts both 'pushed' migration eastward and 'pulled' successful eastern settlement.

Formed by the convergence of Western Pacific westerlies and the easterly trade winds of the Central and Eastern Pacific, and triggered by atmospheric Rossby waves, the South Pacific Convergence Zone (SPCZ) is the main source of precipitation for 10 million people living across numerous islands in the Southern Pacific Ocean. Changes in the El Niño–Southern Oscillation (ENSO), which affects the east–west distribution of rain across the SPCZ, can lead to multi-annual droughts that have in the past devastated human populations[1] and likely triggered Polynesian migration[2]. The future impacts of anthropogenic climate change on Pacific hydroclimate are poorly constrained[3], likely due to systematic model biases in coupled ocean-atmosphere models[4] in addition to uncertainty in the projections of Pacific sea surface temperature (SST) gradients[5].

The state of the tropical Pacific Ocean, which affects the position of the SPCZ, is uncertain and contested over the past 1500 years[6]. Whilst some tropical hydroclimate reconstructions indicate trends consistent with a move towards more El Niño-like conditions[7,8] others indicate the opposite[9,10]. However, proxy records of SST indicate a weakening of the zonal SST gradient[11,12] i.e. a transition from La Niña-like to El Niño-like. In the SPCZ region of the tropical South Pacific, dynamical analysis highlights the importance of absolute SST and zonal SST gradients on precipitation[3,13]. Thus, if the mean state of the tropical Pacific changed from a La Niña- to El Niño-like state, we might expect a northeastern shift in the SPCZ rainfall

patterns, similar to those that occur during El Niño events, influencing food and water security for human populations in this region, and potentially facilitating migration into Eastern Polynesia from around 1000 years BP[2]. To date, the evidence for such hydroclimate changes over the past few millennia has been limited to the South-West and Central SPCZ regions e.g.[14] and missing from the South-East SPCZ. In addition, coupled climate model simulations of the last 1000 years do not reproduce the observed SST trends in the Pacific Ocean.

By applying a combination of palaeoclimate records and novel model simulations we can determine the response of the SPCZ to Pacific mean state changes beyond instrumental time periods and sampling locations. This can also offer insights into the sensitivity of the SPCZ to anthropogenic climate change by exploring the mechanisms that have driven its variation over the past 1–2 millennia. However, both climate proxies and model simulations are challenging to interpret in the SPCZ region. Whilst proxy reconstructions, notably from coral and speleothem archives, have revealed decadal variability to SPCZ movements[15,16], the present low number of climate archives and uncertainties about long-term controls on proxy signals[17] are strong limitations. Likewise, the coupled ocean–atmosphere models used in many studies exhibit systematic 'double-ITCZ' biases in the orientation of the SPCZ, caused by poor simulation of the energy flux into the Southern Hemisphere atmosphere[18]. It is difficult, therefore, to identify climatic

[1]School of Geography and Environmental Science, University of Southampton, Southampton, UK. [2]Climatic Research Unit, University of East Anglia, Norwich, UK. [3]School of Environmental Sciences, University of East Anglia, Norwich, UK. [4]School of Ocean and Earth Science, University of Southampton, Southampton, UK. [5]School of Engineering, Mathematics and Physics, University of East Anglia, Norwich, UK. [6]These authors contributed equally: Mark Peaple, Daniel T. Skinner. ✉e-mail: M.D.Peaple@soton.ac.uk

controls on the SPCZ with either approach individually[19]. In particular, climate model simulations of the last millennium typically do not exhibit any notable centennial-scale trends in tropical Pacific SST[12].

Here, we employ a multidisciplinary approach, involving both proxies and climate models, to resolve centennial- to millennial-scale variations in the SPCZ and their causes. For our proxy analysis, we have produced two new 2000-year-long plant wax stable hydrogen isotope records from Tahiti and Nuku Hiva, French Polynesia. We combine these with previously published biomarker and Ti records that have been interpreted as primarily reflecting changes in hydroclimate (Fig. S4) and use Monte Carlo Empirical Orthogonal Function (MCEOF) analysis[20] to isolate their leading mode of variability whilst taking into account time and proxy uncertainty. The approach allows for the first time, a robust reconstruction of temporal and spatial patterns of precipitation across the SPCZ change over the last 1500 years.

To investigate the potential drivers of centennial- and millennial-scale precipitation changes in the SPCZ we use a global circulation model (IGCM4)[21] forced by different SST patterns. IGCM4 accurately represents the diagonal orientation of modern SPCZ precipitation[13], and, being an atmosphere-only model, does not exhibit the 'double-ITCZ' bias that is present in most coupled climate models[22–24].

Results and discussion
Reconstructing SPCZ precipitation change
Our knowledge of long-term precipitation change across the SPCZ is constrained by limited multi-centennial hydroclimate proxy reconstructions[25], especially in the eastern SPCZ, which is heavily impacted by extreme El Niño events[26]. We therefore generated two new hydroclimate records[27] from peat cores sampled in Tahiti (French Polynesia, 17.6638°S, 149.4218°W), and Nuku Hiva (French Polynesia, 8.868750°S, 140.137500°W; Fig. 1) using plant wax n-alkanes (Fig. 2), to better constrain

changes in the central and eastern SPCZ precipitation over the past 2000 years (2000–100 years BP). Core NHS-2A is characterised by a homogenous organic carbon-rich peat sequence. Total organic carbon (TOC) was consistently high (mean = 41.8%) throughout the profile (Fig. S2). Visually, the core is a dark brown, homogenous, and well-decomposed amorphous peat, particularly in the upper 40 cm. The presence of intermittent fibrous material indicates the preservation of plant macrofossils. Together, these traits suggest a relatively stable depositional environment. Core TAH-A is also composed of organic carbon-rich peat (mean TOC = 75%), but its stratigraphy reveals evidence of environmental disturbance. The majority of the core consists of very dark amorphous peat with visible plant macrofossils. However, a distinct decrease in TOC (77–43%) occurs between 83–103 cm, indicating a notable increase in minerogenic content. Given the core's proximity to the caldera sidewall, this layer is interpreted as an intercalated colluvial deposit. This feature likely represents an allochthonous influx of sediment from a mass movement event on the adjacent slopes, which temporarily interrupted autochthonous peat accumulation.

In the low latitudes, the stable hydrogen isotopic composition (δ^2H) of precipitation is negatively correlated with precipitation rate, a phenomenon known as the 'amount affect'. This relationship has been robustly demonstrated within the SPCZ zone through both isotope-enabled models[28] and direct measurement of meteoric waters[29]. We confirm that this relationship holds at our core sites by comparing precipitation rate data (GPCP) with interpolated δ^2H of precipitation (OIPC), which shows a similar negative correlation (Fig. S3).

To reconstruct past changes in precipitation, we use the δ^2H of higher plant leaf waxes (plant wax δ^2H). Plant wax δ^2H is locally responsive to changes in precipitation δ^2H in tropical forests soils and vegetation[30], lake sediments[31], marine environments[32] and peats[33]. As such, plant wax δ^2H are a well-established proxy for reconstructing past hydroclimate dynamics across various environments and timescales. We find that from 1000 years
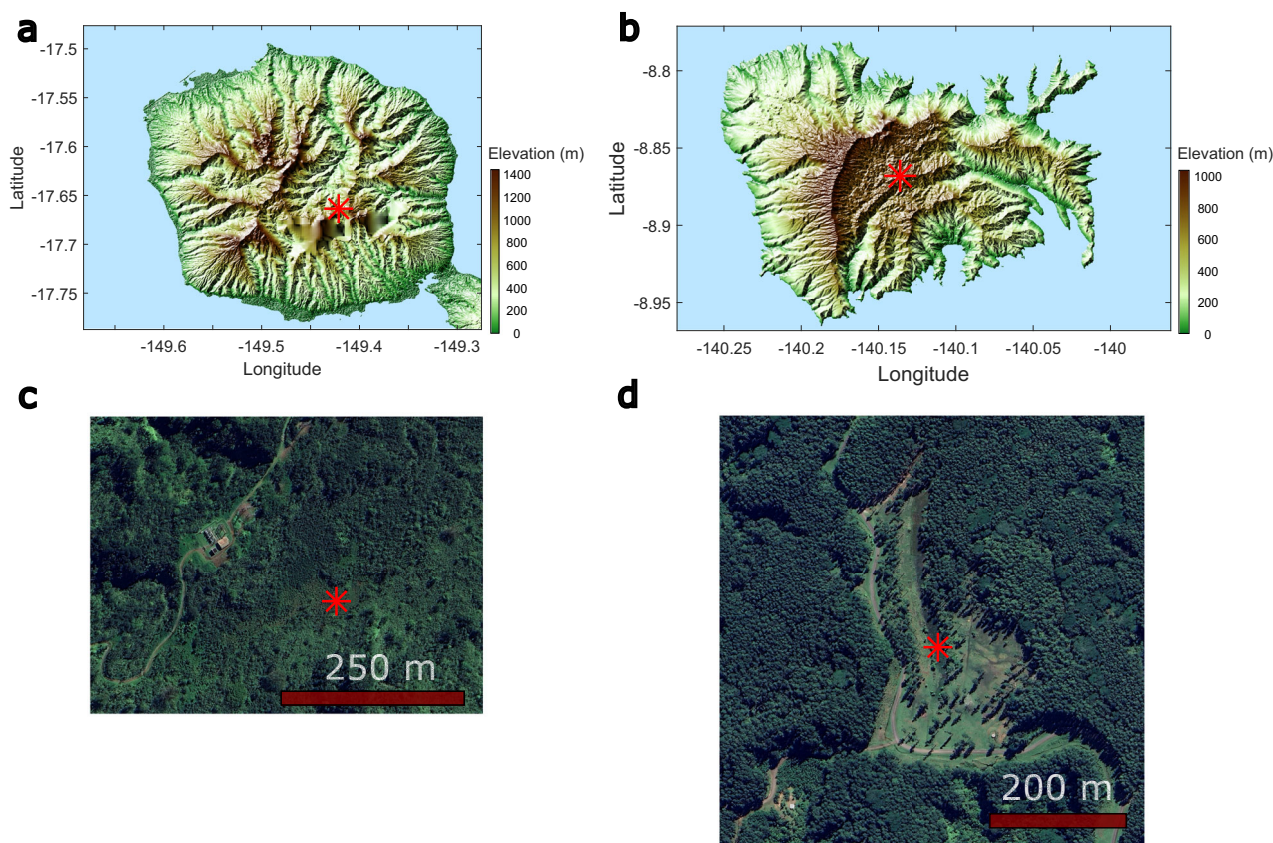

Fig. 1 | Locations of the sediment core sites. a Overview map of site TAH-A in Tahiti and **b** site NHS-2 in Nuku Hiva. The digital elevation model is the 30 m Copernicus DEM. **b**, **c** Corresponding high-resolution satellite imagery for each site, obtained from Google Earth Pro.

BP to present, plant wax δ^2H from both Tahiti and Nuku Hiva becomes more negative (by ~10‰ in both cases), suggesting a wetting trend in Eastern Polynesia. A positive trend in precipitation across Eastern Polynesia is supported by our new proxy evidence, which is marked on Fig. 2. Marshes formed at the T'oovi plateau, Nuku Hiva, between 800–700 years BP[17], likely driven by increased rainfall. Likewise, an increase in pollen abundance from 400 years BP to present suggests a further increase in precipitation[17]. Whilst changes in vegetation composition can also impact plant wax δ^2H[34], vegetation composition shows little variation over the past 700 years[17], despite an overall increase in pollen abundance. Furthermore, the relatively high-altitude locations of our sites in both Tahiti (680 m) and Nuku Hiva (845 m) are remote from historical and modern population centres, making a substantial anthropogenic influence on the proxy records through land-use change unlikely. In Tahiti, diatom evidence from Lake Vaihiria indicates
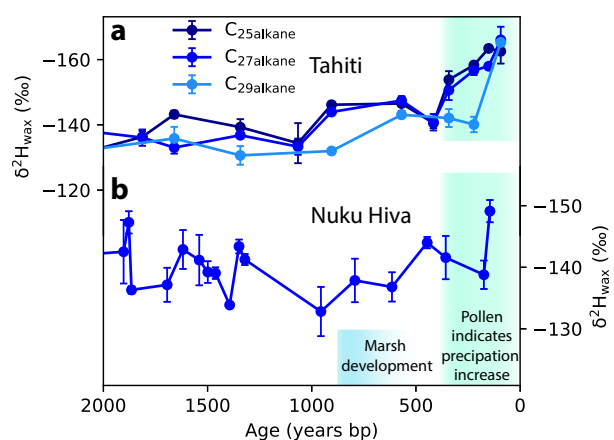
that water depth increased between 350–150 years BP, driven by an increase in precipitation[35]. A long-term trend of increasing precipitation post-1000 years BP was previously identified in a marine core record proximal to Tahaa (Fig. S4) capturing changes in terrestrial Ti input[25].

To generate robust reconstructions of spatial patterns in past precipitation change across the whole SPCZ region, we identified proxy sites that are not influenced by human land use changes (Fig. 3 and see 'Methods'), and performed MCEOF analysis on two independent groups of proxies: the hydrogen isotopic composition of organic biomarkers (n-alkanes and dinosterol) and the Ti content of peat/lake sediments, where more Ti indicates greater runoff and thus wetter conditions[36]. Both of the leading principal components in our biomarker and Ti MCEOF analysis show a trend between 1100 years BP and 400 years BP (Fig. 3a, b) that extends to 200 years BP for the sites where we used biomarkers. This temporal trend is associated with increasingly wetter conditions inferred for the eastern sites and progressively drier conditions for the western sites, consistent between the two proxy types (based on the loading pattern of the EOFs across both biomarker and Ti MCEOFs: Fig. 3c, d). Agreement in the respective first principal components and EOF loading patterns for both biomarker and Ti proxies provides confidence that they are responding to a common hydroclimatic forcing.

Across both proxy MCEOFs we find the greatest agreement in the EOF loading pattern for the easternmost (Tahaa/Tahiti/Nuku Hiva—positive loading) and westernmost (Efate—negative loading) sites in our reconstructions (Fig. 3). The central sites ('Upolu and 'Uvea) show more variance in their association with PC1. At 'Upolu biomarker and Ti MCEOFs are of opposite sign, whilst 'Uvea exhibits a high degree of variance due partly to the low amplitude of the proxy signal[29], indicating that changes in hydroclimate here were smaller than at the other islands. Additionally, the 'Upolu Ti record may at times have been modulated by lake level change[29], distorting its hydroclimate signal.

Taken together, multiple lines of evidence indicate an increase in wetness across the Eastern SPCZ region from 1100 to 100 years BP. When added to evidence from the western SPCZ region, an ENSO-like dipole pattern in SPCZ hydroclimatic change emerges across at least 1100 to 400 years BP, consisting of drying in the western SPCZ and an increase in wetness in the eastern SPCZ region.

Fig. 2 | Newly collected plant wax hydrogen isotope records as proxies for precipitation in French Polynesia. Plant wax n-alkane hydrogen isotope records from a Tahiti and b Nuku Hiva. Error bars show analytical uncertainty (1 standard deviation). Blue shading represents the initiation of marsh development on Nuku Hiva[17] and green shading represents increases in pollen abundance in Nuku Hiva[17] and an increase in deep water adapted diatoms in Tahiti[35].
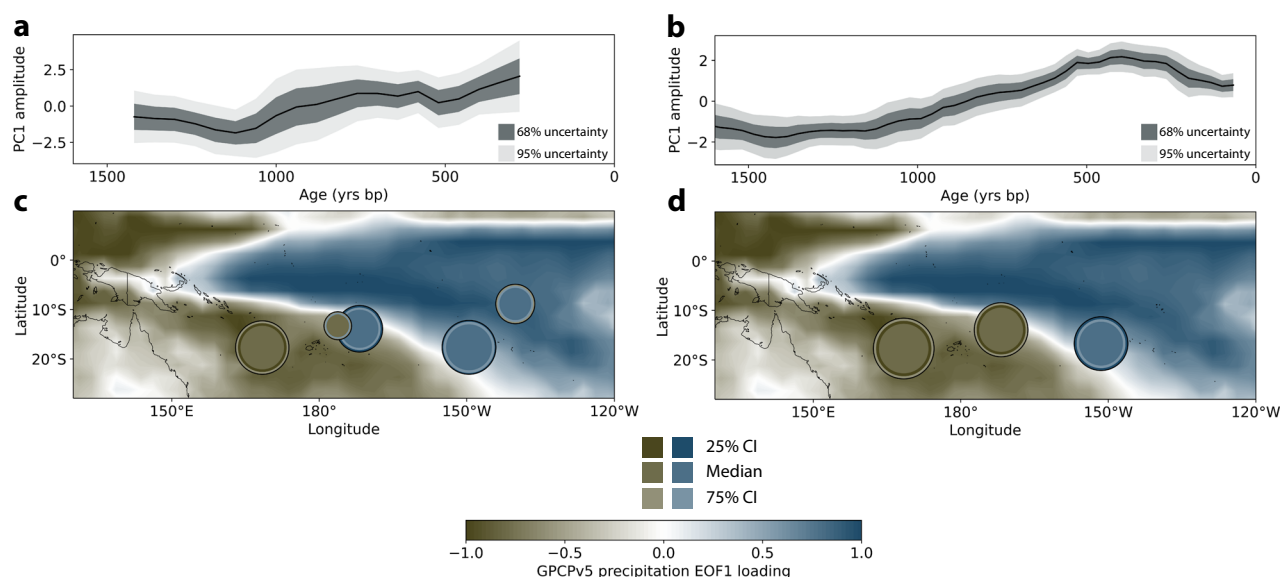

Fig. 3 | Dominant spatial and temporal pattern of precipitation in the SPCZ region during the last 1500 years. First principal component of biomarker and Ti hydroclimate proxy time series (a, b) and EOF loadings (circles in c, d) on individual proxy sites shown with the first EOF (a spatial signal of ENSO) of modern winter precipitation (Global Precipitation Climatology Project 2.3[72]) in the background.

The median EOF loading value is indicated by circle diameter and colour of the inner circle (brown negative, blue positive). Uncertainty (including age model and proxy analytical errors) is indicated for the loading values by the colours of the middle circle (0.25 quantile) and outer circle (0.75 quantile) and for the principal component time series by the dark and light grey shading.
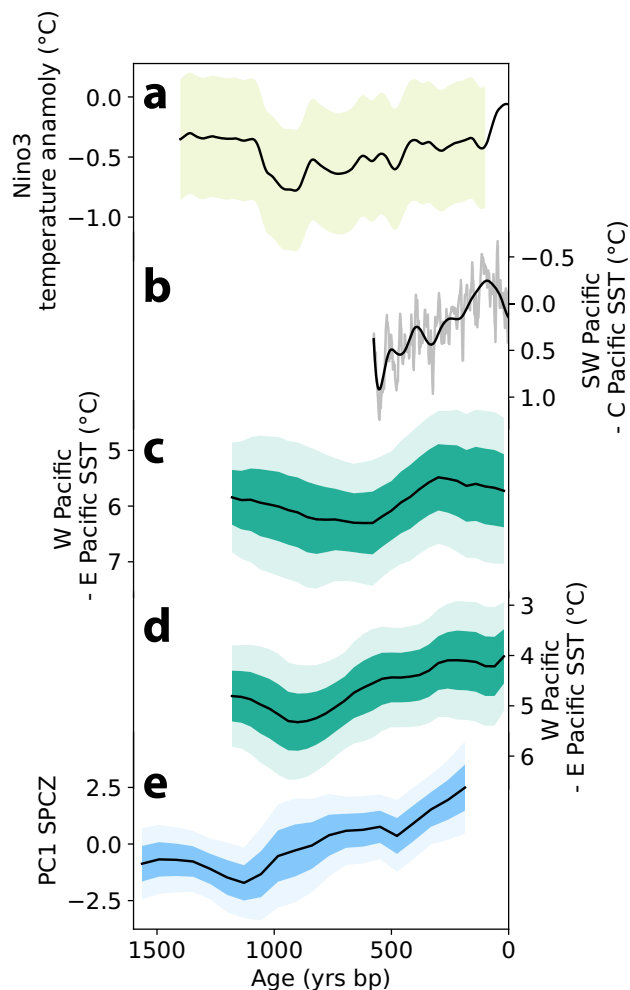
Fig. 4 | Comparison of reconstructed tropical Pacific zonal SST gradient and dominant mode of SPCZ precipitation change. a Reconstruction of ENSO strength based on ENSO sensitive proxies[39] smoothed to show centennial and longer trends. The shaded area is the 95% confidence interval. **b** Pacific South-West minus Central Pacific SST gradient[12]. **c, d** Pacific West minus East SST gradient calculated as a Western Pacific SST compilation[41] revised using the Bacon age model package[50] minus Eastern Pacific SST from ref. 40 (**c**) or ref. 73 (**d**), with 1 and 2 standard deviation age uncertainties shaded. **e** Principal component 1 of hydroclimate bio-marker proxies in the SPCZ (this study), with 1 and 2 standard deviation uncertainties shaded. The y-axis scales have been reversed in (**b, c, d**) to aid interpretation.

The effects of past changes in the tropical Pacific zonal SST gradient

The position of the SPCZ is sensitive to the zonal gradient of SSTs across the tropical Pacific[13,37]. We therefore compare our biomarker and independent Ti proxy PC1 from the SPCZ (Fig. 3a) to proxy reconstructions of ENSO and of the east–west (i.e. zonal) tropical Pacific SST gradient (Fig. 4). Reconstructions[7] indicate both increased ENSO variance[38] and a shift from a La Niña-like state to a more ENSO-neutral state over the past 1100 years (Fig. 4a)[39]. These reconstructions align with changes in the SST gradient across the Pacific basin (Fig. 4c, d)[40,41], which show a decreased east–west SST gradient since 1000 years BP.

We link the spatio-temporal changes in hydroclimate revealed by our proxy network to changes in tropical Pacific SST gradients using simulations with the IGCM4 global atmospheric circulation model. These simulations are designed to explore potential changes in the last 1000 years, but before the appearance of a global anthropogenic climate change signal.

The two experiments use pre-industrial atmospheric composition but differ in the SST fields used as the lower boundary condition. In the present-

day experiment (*PRE* hereafter), the SST fields (Fig. 5c) represent those around 1900 CE (see Methods). The SST fields for the 1000 yrs BP experiment (*1KBP* hereafter) are perturbed to strengthen the zonal SST gradient in the tropical Pacific that likely prevailed around that time (Fig. 5a).

To ensure that the perturbed SST fields remain dynamically/physically plausible, we apply an SST change pattern calculated as the first empirical orthogonal function (EOF) of decadal-scale SST variability over the Pacific basin simulated by coupled climate models. Specifically, it is the multi-model mean representation of decadal pan-Pacific SST variability diagnosed from the pre-industrial control experiments of nine CMIP6 coupled climate models. This EOF pattern closely resembles the Inter-decadal Pacific Oscillation (IPO)[42,43], featuring a change of the tropical Pacific zonal SST gradient whilst also capturing the wider changes in Pacific SSTs coincident with such a zonal gradient change.

This SST anomaly pattern is scaled by a factor of—5 to represent a strengthened tropical Pacific zonal SST gradient that is similar in magnitude to the change shown in proxy reconstructions (Fig. 4b–d) and added to the *PRE* SST field to obtain the *1KBP* SSTs. The zonal SST gradient (between boxes 115–125°W and 90–105°E, each spanning 0–8°S) is approximately 0.6°C weaker in the *PRE* than *1KBP* experiments, which is consistent with the magnitude of gradient change from 1100–200 years BP in Fig. 4. The SST changes from *1KBP* to *PRE* (Fig. 5e) show a warming in the central/eastern Pacific as the east-west gradient weakens.

Whilst the SPCZ is strongest in boreal winter, we present annual averages to facilitate comparison with proxy reconstructions which reflect an annual mean signal. From the *1KBP* simulation (Fig. 5b) to the *PRE* simulation (Fig. 5d) the SPCZ shifts north-eastwards (Fig. 5f), with drying of the south-western SPCZ and wetting of the north-eastern SPCZ. The stronger tropical zonal SST gradient in the *PRE* simulation leads to stronger easterly trade winds and an enhanced Walker Circulation, also producing an increase in precipitation over the western tropical Pacific. This pattern of change is strikingly similar to the changes exhibited by our proxy net-work (Fig. 3).

The mechanism linking the SST gradient change to the SPCZ response is as follows: warmer SSTs in the eastern South Pacific and cooler SSTs in the western South Pacific shift moisture availability north-eastwards. Rossby waves entering the SPCZ region therefore propagate further to the north-east before the associated vorticity anomalies are able to trigger deep convection[37]. The result is a reduction in deep convection and precipitation over the western South Pacific, and an increase in precipitation over the eastern South Pacific.

SPCZ hydroclimatic changes and their implications

Proxy reconstructions of precipitation in the SPCZ (Fig. 3) show a trend of drying in the western South Pacific and wetting in the eastern South Pacific over the past 1000 years, which indicates an eastward shift in the SPCZ. This is consistent with our modelling results (Fig. 5f) which suggest the shift in the SPCZ over the past 1000 years could have been driven by concurrent weakening of the tropical Pacific zonal SST gradient (Fig. 4). These observations lend independent support to Jiang et al. and D'Olivo et al.[7,12] reconstructions of wider equatorial mean Pacific state change over this period and strengthen the argument for a transition in mean SPCZ state from La Niña-like to relatively more El Niño-like rainfall patterns characterised by a trend towards drier conditions in the south western SPCZ, and wetter in the eastern SPCZ.

Hydroclimatic changes in the SPCZ region may have had wide-reaching implications, including major impacts on the human settlement of Polynesia. The final expansion by humans into Eastern Polynesia around 1000 years BP followed an ~1700-year pause during which distinct Polynesian culture developed in the islands of Samoa and Tonga[44]. The drivers of the final eastward expansion into the Pacific are debated, with technological[45], cultural, and climatic factors[2] being proposed. A long-term drought in western Polynesia between 1100 and 800 years BP was previously suggested as a 'push factor' for migration[2]. Our MCEOF analysis confirms
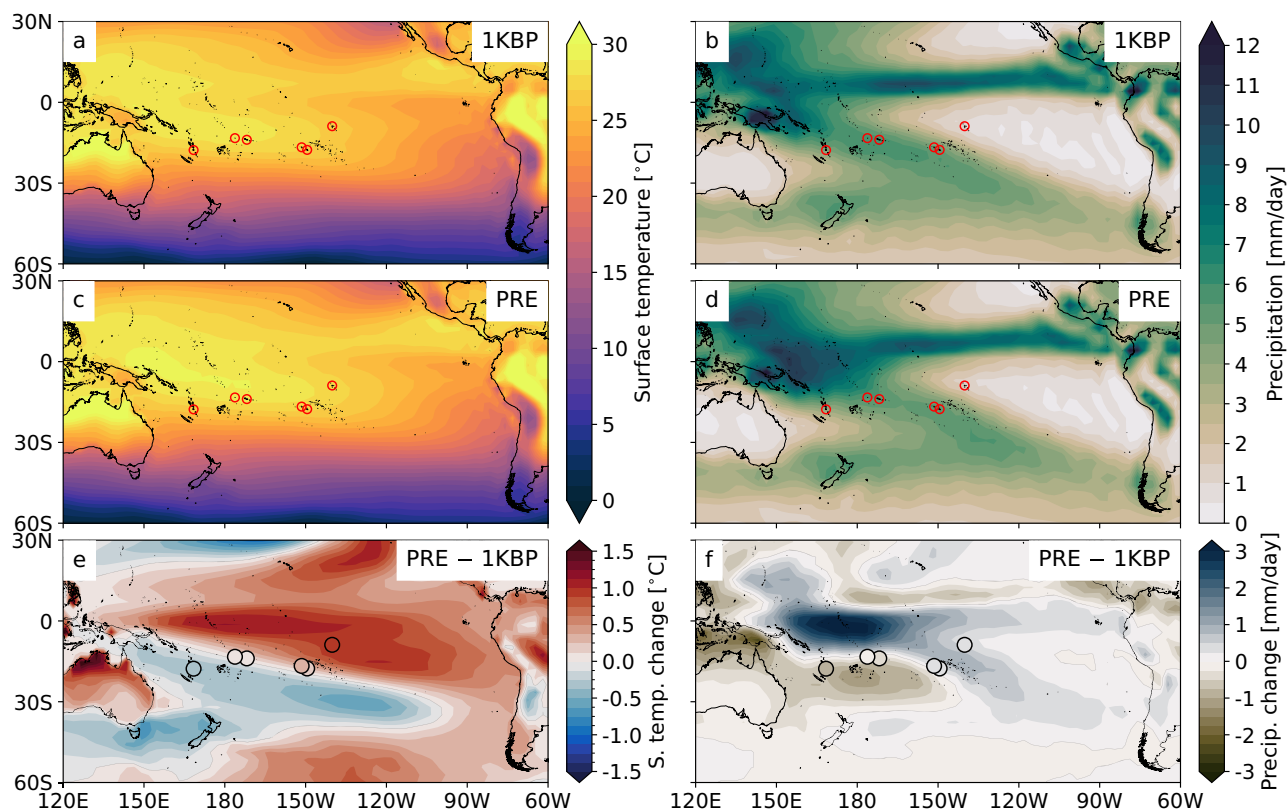
Fig. 5 | Climate model simulations of temperature and precipitation over the last 1000 years. (**a**, **c**) Mean surface temperature and (**b**, **d**) mean precipitation simulated by IGCM4 for the *1KBP* (**a**, **b**) and *PRE* (**c**, **d**) experiments. The implied change in mean surface temperature (**e**) and precipitation (**f**) from 1000 years BP to present (i.e. *PRE* minus *1KBP*; thin grey line is the zero change contour). The locations of Efate, 'Uvea, 'Upolu, Tahiti, Tahaa, and Nuku Hiva are marked, from West to East, by the red circles in (**a**–**d**), and by filled circles showing the simulated change in mean temperature (**e**) and precipitation (**f**) at each island location.

that drying occurred in western Polynesia around the time of the migration, and our hydroclimate proxy records reveal that this coincided with increased precipitation in Eastern Polynesia (the IGCM experiments show >40% increase in Nuku Hiva), thus serving as a 'pull factor' for migration and supporting settlement in the eastern island archipelagos. Our climate modelling shows that these contrasting western and eastern Polynesia trends did not occur together by chance, but were likely driven by a dynamical response to the change in zonal SST gradients in the tropical Pacific. In addition, the decrease in trade wind strength associated with a shift away from a La Niña-like mean state after 1000 years BP would have increased the success of canoes travelling from western to eastern Polynesian islands[46].

Finally, recent work has highlighted how coupled climate models might not accurately simulate current and future changes in the zonal SST Pacific gradient[5,47] due to poorly constrained eastern Pacific cooling[48]. Our work demonstrates how accurate projections of this SST gradient are of vital importance in predicting future precipitation changes in a region already heavily impacted by anthropogenic climate change.

Methods
Site information, sediment coring and age modelling
We collected sediment cores from Moūku Swamp, Nuku Hiva (core NHS-2) and Anaorii Plateau, Tahiti (core TAH-A), using a Russian Corer (Fig. 1). Tahiti core TAH-A was collected on 19th September 2022 from Anoroi'i Swamp, under the headwall of Papeno'o Valley at an altitude of 685 m. Anoroi'i Swamp was formed on the back slope of a large slip, in an area of impeded drainage. Vegetation is dominated by *Cyclosorus* ferns (*interruptus* spp), and Pandanus forest. Nuku Hiva core NHS-2 was collected on 6th September 2022 from Moūku Swamp, a 400 × 50 m ribbon swamp located on the To'ov'i plateau, a highland formed through a caldera collapse in the centre of the island. Modern vegetation is heavily impacted by

anthropogenic activities and consists of Pine trees along swamp banks and grass (Setaria, Paspallum, Wedelia), sedges (Pycreus, Fimbristylis, Cyperus, Kyllenga) and herbs (Ageratum, Centella) dominating the swamp vegetation assemblage. Both cores were generated by aligning separate core segments using elemental data derived from X-ray fluorescence analysis in addition to sediment colour and water content percentage. After collection, cores were transported to the University of Southampton School of Geography and Environmental Science and kept refrigerated at 5 °C. To generate an age model, we radiocarbon-dated organic material (bulk and macro fossil) sampled from both cores using accelerated mass spectrometry (AMS). We generated seven ^{14}C dates from the NHS-2 core and seven ^{14}C dates from the TAH-A core. Radiocarbon dates were calibrated using SHCal20[49] and then a Bayesian age model was constructed using the R package Bacon[50] (Fig. S1).

Lipid extraction and hydrogen isotope analysis. We collected sediment from Nuku Hiva core NHS-2 ($n = 18$) and from Tahiti core TAH-A ($n = 12$), resulting in average sampling resolutions of 111 years and 167 years, respectively. Approximately 3–6 g of sediment was dried, ground, and extracted using a Dionex Accelerated Solvent Extraction system at the University of Southampton. Extraction was carried out with a 9:1 mixture of dichloromethane (DCM) and methanol (MeOH) at 100 °C and 1500 psi to produce the total lipid extract (TLE).

The TLE was then fractionated into neutral and acidic components using NH$_2$ sepra bulk packing columns. The neutral fraction was isolated with a 2:1 DCM:isopropanol mixture and further refined through silica gel column chromatography. *n*-alkanes were separated using hexane as the eluent. Prior to gas chromatography (GC) analysis, the *n*-alkanes were treated with copper to remove elemental sulphur. Identification and quantification of *n*-alkanes was performed using a Thermo Trace 1310 GC

system (60 m column) equipped with a flame ionisation detector (GC-FID), with results verified against an in-house standard containing known concentrations of *n*-alkanoic acids and *n*-alkanes.

To infer past hydroclimate variability, we analysed the hydrogen isotopic composition (δ^2H_{wax}) of plant waxes, focusing on *n*-alkanes (C_{27} and C_{29}). Measurements were conducted with a Thermo Trace 1310 GC (Restek column: 30 m × 0.25 mm × 0.1 μm) linked to a Thermo Scientific Delta V Plus isotope ratio mass spectrometer via a GC Isolink interface with a pyrolysis furnace (1400 °C). Quality control included daily monitoring of δ^2H linearity using H_2 reference gas, recording an average H^+ factor of 2.59 ppm/mV. Calibration was performed daily using a standard mixture (C_{17}–C_{25} *n*-alkanes, A6 mix from A. Schimmelmann, University of Indiana) with δ^2H values ranging from −17‰ to −256‰, achieving a mean peak RMS of 1.7‰. δ^2H values were normalised to Vienna Standard Mean Ocean Water and Vienna Pee Dee Belemnite standards.

MCEOF analysis
We followed the method of Anchukaitis and Tierney[20] to perform our MCEOF analysis. Briefly, we recalculated age models using the R package Bacon[50] for each proxy time series. We then randomly selected one age model ensemble member for each proxy and interpolated each proxy's time series to a common time step. We then performed a principal component analysis on the correlation matrix of *z*-scored time series. We repeated this process 4000 times generating distributions of principal component loadings and time series. To calculate statistics on the first principal component time series we binned the data along the time axis and calculated the mean and standard deviation of each bin.

The IGCM4 model and experimental design
Modelling experiments were run with the Intermediate General Circulation Model, version 4 (IGCM4)[21], an atmosphere–only spectral primitive equation model. The configuration used here has a spectral truncation of T42 (~2° horizontal resolution in the tropics), and is run on 35 model levels (which includes a fully resolved stratosphere). Convection is parameterised by the scheme of Forster et al.[51], with separate handling of deep and shallow convection. Model experiments were run for 100 years, with the final 80 years analysed to allow for 20 years of spinup.

The pre-industrial SST climatology used in the *PRE* experiment (Fig. S6) was generated by taking the mean (by month of the year) of 1880–1920 SST data from the 20th Century Reanalysis product, version 2[52]. Greenhouse gas concentrations were fixed at pre-industrial levels (CO_2, NH_4 and N_2O at 280 ppm, 720 ppb, and 285 ppb, respectively).

The pre-industrial control simulations of nine CMIP6 coupled climate models were used to create a physically and dynamically realistic global map of SST anomaly associated with a change to the tropical Pacific zonal SST gradient (for the *1KBP* experiment). These models are:
- ACCESS ESM1.5[53,54]
- CanESM5[55,56]
- CESM2[57,58]
- FGOALS-g3[59,60]
- GISS E2.1G[61,62]
- IPSL–CM6AL–LR[63,64]
- MIROC6[65,66]
- MPI ESM1.2–LR[67,68]
- UKESM1.0–LL[69,70]

The models were chosen by applying four criteria, based on those used by Coburn and Pryor[71] in their review of different modes of variability in CMIP6:
- Monthly SST, sea level pressure, and 500-hPa geopotential height data are available (sea level pressure and geopotential height data used for diagnostics not presented here).
- The chosen subset of models should capture the range of horizontal resolutions and equilibrium climate sensitivities found across CMIP6.

- Models should be independent of each other (although ACCESS ESM1.5 and UKESM1.0–LL share the same ocean model they have different representations of the atmosphere).
- The first empirical orthogonal function (EOF) of decadally-smoothed Pacific SSTs should correspond to variability in the tropical Pacific zonal SST gradient (i.e. the IPO).

For each model, the first EOF of 10-year low-pass filtered, monthly averaged SST anomalies was calculated over the Pacific basin and its corresponding principal component time series was then normalised to unit variance. To capture physically realistic annual cycles of the SST changes, SST anomaly data from each model were then subset by month of the year and 10-year low-pass filtered (i.e. a 10-point low pass filter of all Januaries, etc.), before being regressed onto the relevant principal component time series to give a global SST anomaly map for each model and month of the year (i.e. 9 models × 12 months = 108 SST anomaly maps). A multi-model mean SST anomaly map was then created for each month by averaging over the nine models (Fig. S7). These SST anomaly maps were multiplied by a factor of minus five to approximately match weakening of the tropical Pacific zonal SST gradient from Fig. 4.

SST fields for the *1KBP* experiment were generated by adding these final SST anomaly maps to the pre-industrial SST climatology used in the *PRE* experiment. The two experiments are in all other ways identical to isolate the effect of the SST gradient change.

Data availability
Proxy data generated as part of this study are available via the Open Science Framework[27]. Reanalysis SST data are from the twentieth century Reanalysis product, version 2[52]. CMIP6 model data used are available via the Earth System Grid Federation[53–70].

References
1. d'Aubert, A. & Nunn, P. D. *Furious Winds and Parched Islands: Tropical Cyclones (1558-1970) and Droughts (1722-1987) in the Pacific* (Xlibris Corporation, 2012).
2. Sear, D. A. et al. Human settlement of East Polynesia earlier, incremental, and coincident with prolonged South Pacific drought. *Proc. Natl Acad. Sci. USA* **117**, 8813–8819 (2020).
3. Brown, J. R. et al. South Pacific convergence zone dynamics, variability and impacts in a changing climate. *Nat. Rev. Earth Environ.* **1**, 530–543 (2020).
4. Dutheil, C. et al. Impact of surface temperature biases on climate change projections of the South Pacific Convergence Zone. *Clim. Dyn.* **53**, 3197–3219 (2019).
5. Wang, Z., Dong, L., Song, F., Zhou, T. & Chen, X. Uncertainty in the past and future changes of tropical Pacific SST zonal gradient: internal variability versus model spread. *J. Clim.* **37**, 1465–1480 (2024).
6. Atwood, A. R., Battisti, D., Wu, E., Frierson, D. & Sachs, J. P. Data-model comparisons of tropical hydroclimate changes over the common era. *Paleoceanogr. Paleoclimatol.* **36**, e2020PA003934 (2021).
7. Jiang, S. et al. The mean state of the tropical Pacific Ocean differed between the medieval warm period and the industrial era. *Commun. Earth Environ.* **4**, 74 (2023).
8. Zhang, J., Liang, M.-Q., Li, T.-Y., Chen, C.-J. & Li, J.-Y. Asian–Australian monsoon evolution over the last millennium linked to ENSO in composite stalagmite δ18O records. *Quat. Sci. Rev.* **281**, 107420 (2022).
9. Yan, H. et al. A record of the Southern Oscillation Index for the past 2,000 years from precipitation proxies. *Nat. Geosci.* **4**, 611–614 (2011).

6

10. Konecky, B. L. et al. Intensification of southwestern Indonesian rainfall over the past millennium. *Geophys. Res. Lett.* **40**, 386–391 (2013).

11. Conroy, J. L., Overpeck, J. T. & Cole, J. E. El Niño/Southern Oscillation and changes in the zonal gradient of tropical Pacific sea surface temperature over the last 1.2 ka. *PAGES News* **18**, 32–34 (2010).

12. D'Olivo, J. P. et al. Coral Sr/Ca-SST reconstruction from Fiji extending to ~1370 CE reveals insights into the Interdecadal Pacific Oscillation. *Sci. Adv.* **10**, eado5107 (2024).

13. van der Wiel, K., Matthews, A. J., Joshi, M. M. & Stevens, D. P. Why the South Pacific Convergence Zone is diagonal. *Clim. Dyn.* **46**, 1683–1698 (2016).

14. Maloney, A. E. et al. Contrasting common era climate and hydrology sensitivities from paired lake sediment dinosterol hydrogen isotope records in the South Pacific Convergence Zone. *Quat. Sci. Rev.* **281**, 107421 (2022).

15. Linsley, B. K. et al. SPCZ zonal events and downstream influence on surface ocean conditions in the Indonesian Throughflow region. *Geophys. Res. Lett.* **44**, 293–303 (2017).

16. Faraji, M. et al. Controls on rainfall variability in the tropical South Pacific for the last 350 years reconstructed from oxygen isotopes in stalagmites from the Cook Islands. *Quat. Sci. Rev.* **289**, 107633 (2022).

17. Allen, M. S., Butler, K., Flenley, J. & Horrocks, M. New pollen, sedimentary, and radiocarbon records from the Marquesas Islands, East Polynesia: implications for archaeological and palaeoclimate studies. *Holocene* **21**, 473–484 (2011).

18. Hwang, Y. T. & Frierson, D. M. Link between the double-Intertropical Convergence Zone problem and cloud biases over the Southern Ocean. *Proc. Natl. Acad. Sci. USA* **110**, 4935–4940 (2013).

19. Wilson, R. et al. Reconstructing ENSO: the influence of method, proxy data, climate forcing and teleconnections. *J. Quat. Sci.* **25**, 62–78 (2010).

20. Anchukaitis, K. J. & Tierney, J. E. Identifying coherent spatiotemporal modes in time-uncertain proxy paleoclimate records. *Clim. Dyn.* **41**, 1291–1306 (2013).

21. Joshi, M., Stringer, M., van der Wiel, K., O'Callaghan, A. & Fueglistaler, S. IGCM4: a fast, parallel and flexible intermediate climate model. *Geosci. Model Dev.* **8**, 1157–1167 (2015).

22. Li, G. & Xie, S.-P. Tropical biases in CMIP5 multimodel ensemble: the excessive equatorial Pacific cold tongue and double ITCZ problems. *J. Clim.* **27**, 1765 – 1780 (2014).

23. Samanta, D., Karnauskas, K. B. & Goodkin, N. F. Tropical Pacific SST and ITCZ biases in climate models: double trouble for future rainfall projections? *Geophys. Res. Lett.* **46**, 2242–2252 (2019).

24. Fiedler, S. et al. Simulated tropical precipitation assessed across three major phases of the Coupled Model Intercomparison Project (CMIP). *Mon. Weather Rev.* **148**, 3653–3680 (2020).

25. Toomey, M. R., Donnelly, J. P. & Tierney, J. E. South Pacific hydrologic and cyclone variability during the last 3000 years. *Paleoceanography* **31**, 491–504 (2016).

26. Kidwell, A., Lee, T., Jo, Y. H. & Yan, X. H. Characterization of the variability of the South Pacific convergence zone using satellite and reanalysis wind products. *J. Clim.* **29**, 1717–1732 (2016).

27. Peaple, M., Inglis, G. N., Sear, D. & Langdon, P. A 2000-Year Record of Plant Wax Hydrogen Isotopes from French Polynesia. https://doi.org/10.17605/OSF.IO/VMK7X (2025).

28. Conroy, J. L., Cobb, K. M. & Noone, D. Comparison of precipitation isotope variability across the Tropical Pacific in observations and swing2 model simulations. *J. Geophys. Res.* **118**, 5867–5892 (2013).

29. Maloney, A. E. et al. Reconstructing precipitation in the tropical South Pacific from dinosterol 2H/1H ratios in lake sediment. *Geochim. Cosmochim. Acta* **245**, 190–206 (2019).

30. Feakins, S. J. et al. Production of leaf wax n-alkanes across a tropical forest elevation transect. *Org. Geochem.* **100**, 89–100 (2016).

31. McFarlin, J. M., Axford, Y., Masterson, A. L. & Osburn, M. R. Calibration of modern sedimentary δ2H plant wax-water relationships in Greenland lakes. *Quat. Sci. Rev.* **225**, 105978 (2019).

32. Bhattacharya, T., Tierney, J. E., Addison, J. A. & Murray, J. W. Ice-sheet modulation of deglacial North American monsoon intensification. *Nat. Geosci.* **11**, 848–852 (2018).

33. Nichols, J., Booth, R. K., Jackson, S. T., Pendall, E. G. & Huang, Y. Differential hydrogen isotopic ratios of sphagnum and vascular plant biomarkers in ombrotrophic peatlands as a quantitative proxy for precipitation–evaporation balance. *Geochim. Cosmochim. Acta* **74**, 1407–1416 (2010).

34. Sachse, D. et al. Molecular paleohydrology: interpreting the hydrogen-isotopic composition of lipid biomarkers from photosynthesizing organisms. *Annu. Rev. Earth Planet. Sci.* **40**, 221–249 (2012).

35. Parkes, A., Teller, J. T. & Flenley, J. R. Environmental history of the Lake Vaihiria drainage basin, Tahiti, French Polynesia. *J. Biogeogr.* **19**, 431–447 (1992).

36. Metcalfe, S. E., Jones, M. D., Davies, S. J., Noren, A. & MacKenzie, A. Climate variability over the last two millennia in the North American monsoon region, recorded in laminated lake sediments from Laguna de Juanacatlán, Mexico. *Holocene* **20**, 1195–1206 (2010).

37. Matthews, A. J. A multiscale framework for the origin and variability of the South Pacific Convergence Zone. *Q. J. R. Meteorol. Soc.* **138**, 1165–1178 (2012).

38. Li, J. et al. Interdecadal modulation of El Niño amplitude during the past millennium. *Nat. Clim. Change* **1**, 114–118 (2011).

39. Mann, M. E. et al. Global signatures and dynamical origins of the Little Ice Age and Medieval Climate Anomaly. *Science* **326**, 1256–1260 (2009).

40. Conroy, J. L. et al. Unprecedented recent warming of surface temperatures in the eastern tropical Pacific Ocean. *Nat. Geosci.* **2**, 46–50 (2009).

41. Oppo, D. W., Rosenthal, Y. & Linsley, B. K. 2,000-year-long temperature and hydrology reconstructions from the Indo–Pacific warm pool. *Nature* **460**, 1113–1116 (2009).

42. Mantua, N. J. & Hare, S. R. The Pacific decadal oscillation. *J. Oceanogr.* **58**, 35–44 (2002).

43. Intergovernmental Panel on Climate Change (IPCC). *Annex IV: Modes of Variability*, 2153–2192 (Cambridge University Press, 2023).

44. Ioannidis, A. G. et al. Paths and timings of the peopling of Polynesia inferred from genomic networks. *Nature* **597**, 522–526 (2021).

45. Kahn, J. G., Buffington, A., Escue, C. & Crabtree, S. A. Social and ecological factors affect long-term resilience of voyaging canoes in pre-contact Eastern Polynesia: a multiproxy approach from the ArchaeoEcology project. *Front. Ecol. Evol.* **9**, 750351 (2022).

46. Dickson, T., Farr, H., Sear, D. & Blake, J. I. R. Uncertainty in marine weather routing. *Appl. Ocean Res.* **88**, 138–146 (2019).

47. Seager, R. et al. Strengthening tropical Pacific zonal sea surface temperature gradient consistent with rising greenhouse gases. *Nat. Clim. Change* **9**, 517–522 (2019).

48. Lee, S. et al. On the future zonal contrasts of equatorial Pacific climate: perspectives from observations, simulations, and theories. *npj Clim. Atmos. Sci.* **5**, 82 (2022).

49. Hogg, A. G. et al. SHCal20 Southern Hemisphere calibration, 0–55,000 years cal BP. *Radiocarbon* **62**, 759–778 (2020).

50. Blaauw, M. & Christen, J. A. Flexible paleoclimate age–depth models using an autoregressive gamma process. *Bayesian Anal.* **6**, 457 – 474 (2011).

51. Forster, P. Md. F., Blackburn, M., Glover, R. & Shine, K. P. An examination of climate sensitivity for idealised climate change experiments in an intermediate general circulation model. *Clim. Dyn.* **16**, 833–849 (2000).

52. Compo, G. P. et al. The Twentieth Century Reanalysis Project. *Q. J. R. Meteorol. Soc.* **137**, 1–28 (2011).

53. Ziehn, T. et al. CSIRO ACCESS-ESM1.5 model output prepared for CMIP6 CMIP piControl, Version 20210316 (Earth System Grid Federation, 2019).

54. Ziehn, T. et al. The Australian Earth System Model: ACCESS-ESM1.5. *J. South. Hemisph. Earth Syst. Sci.* **70**, 193–214 (2020).

55. Swart, N. C. et al. CCCma CanESM5 model output prepared for CMIP6 CMIP piControl, Version 20190429 (Earth System Grid Federation, 2019).

56. Swart, N. C. et al. The Canadian Earth System Model version 5 (CanESM5.0.3). *Geosci. Model Dev.* **12**, 4823–4873 (2019).

57. Danabasoglu, G., Lawrence, D., Lindsay, K., Lipscomb, W. & Strand, G. NCAR CESM2 model output prepared for CMIP6 CMIP piControl, Version 20190320 (Earth System Grid Federation, 2019).

58. Danabasoglu, G. et al. The Community Earth System Model version 2 (CESM2). *J. Adv. Model. Earth Syst.* **12**, e2019MS001916 (2020).

59. Li, L. CAS FGOALS-g3 model output prepared for CMIP6 CMIP piControl, Version 20191126 (Earth System Grid Federation, 2019).

60. Li, L. et al. The flexible global ocean–atmosphere–land system model grid-point version 3 (FGOALS-g3): description and evaluation. *J. Adv. Model. Earth Syst.* **12**, e2019MS002012 (2020).

61. NASA Goddard Institute for Space Studies (NASA/GISS). NASA-GISS GISS-E2.1G model output prepared for CMIP6 CMIP piControl, Version 20180824 (Earth System Grid Federation, 2018).

62. Kelley, M. et al. GISS-E2.1: configurations and climatology. *J. Adv. Model. Earth Syst.* **12**, e2019MS002025 (2020).

63. Boucher, O. et al. IPSL IPSL-CM6A-LR model output prepared for CMIP6 CMIP piControl, Version 20200326. (Earth System Grid Federation, 2018).

64. Boucher, O. et al. Presentation and evaluation of the IPSL-CM6A-LR climate model. *J. Adv. Model. Earth Syst.* **12**, e2019MS002010 (2020).

65. Tatebe, H. & Watanabe, M. MIROC MIROC6 model output prepared for CMIP6 CMIP piControl, Version 20200326 (Earth System Grid Federation, 2018).

66. Tatebe, H. et al. Description and basic evaluation of simulated mean state, internal variability, and climate sensitivity in MIROC6. *Geosci. Model Dev.* **12**, 2727–2765 (2019).

67. Wieners, K.-H. et al. MPI-M MPI-ESM1.2-LR model output prepared for CMIP6 CMIP piControl, Version 20190710 (Earth System Grid Federation, 2019).

68. Mauritsen, T. et al. Developments in the MPI-M Earth System Model version 1.2 (MPI-ESM1.2) and its response to increasing CO_2. *J. Adv. Model. Earth Syst.* **11**, 998–1038 (2019).

69. Tang, Y. et al. MOHC UKESM1.0-LL model output prepared for CMIP6 CMIP piControl, Version 20200828 (Earth System Grid Federation, 2019).

70. Sellar, A. A. et al. UKESM1: description and evaluation of the U.K. Earth System Model. *J. Adv. Model. Earth Syst.* **11**, 4513–4558 (2019).

71. Coburn, J. & Pryor, S. C. Differential credibility of climate modes in CMIP6. *J. Clim.* **34**, 8145–8164 (2021).

72. Adler, R. F. et al. The Global Precipitation Climatology Project (GPCP) monthly analysis (new version 2.3) and a review of 2017 global precipitation. *Atmosphere* **9**, 138 (2018).

73. Rustic, G. T., Koutavas, A., Marchitto, T. M. & Linsley, B. K. Dynamical excitation of the tropical Pacific Ocean and ENSO variability by little ice age cooling. *Science* **350**, 1537–1541 (2015).

Author contributions
All authors contributed to the conceptualisation of the study. D.S. supervised the project. M.P. and D.T.S. contributed equally to this work; they performed data acquisition and analysis, curated the data and led the writing of the paper. D.S., P.L., M.J. and T.J.O. also contributed to data acquisition. Funding for the project was acquired by D.S., G.N.I., M.J., P.L., A.J.M. and T.J.O. All authors contributed to the editing and review of the final manuscript.

Competing interests
The authors declare no competing interests.

Additional information
Supplementary information The online version contains supplementary material available at https://doi.org/10.1038/s43247-025-02676-5.

Correspondence and requests for materials should be addressed to Mark Peaple.

Peer review information *Communications Earth & Environment* thanks Juan Pablo D'Olivo and the other anonymous reviewer(s) for their contribution to the peer review of this work. Primary handling editors: Yiming Wang and Aliénor Lavergne. A peer review file is available.

Reprints and permissions information is available at http://www.nature.com/reprints

Publisher's note Springer Nature remains neutral with regard to jurisdictional claims in published maps and institutional affiliations.